# Supplementary Information

# A non-Newtonian fluid quasi-solid electrolyte designed for long life and high safety Li-$O_2$ batteries

*Guangli Zheng* [1], *Tong Yan* [1], *Yifeng Hong* [2], *Xiaona Zhang* [1], *Jianying Wu* [2], *Zhenxing Liang* [1], *Zhiming Cui* [1], *Li Du* [1], *Huiyu Song* [1,] *

[1]Guangdong Provincial Key Laboratory of Fuel Cell Technology, School of Chemistry and Chemical Engineering, South China University of Technology, Guangzhou 510641, China

[2]Department of Civil Engineering, South China University of Technology, Guangzhou 510641, China

*Email: hysong@scut.edu.cn

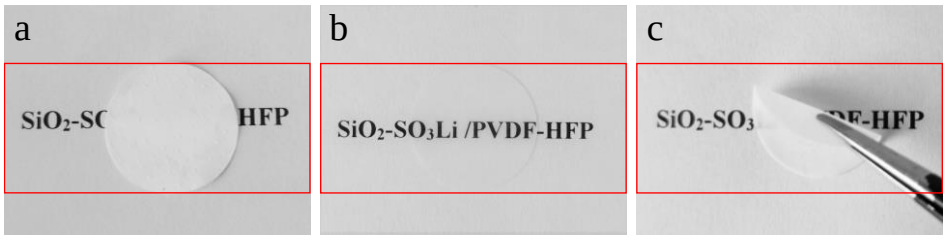


**Supplementary Fig. 1 Digital photos of $SiO_2$-$SO_3Li$/PVDF-HFP a** before and **b** after dipping in liquid electrolyte, and it turns transparent after absorbing liquid electrolyte; **c** It remains flexible after bending several times.

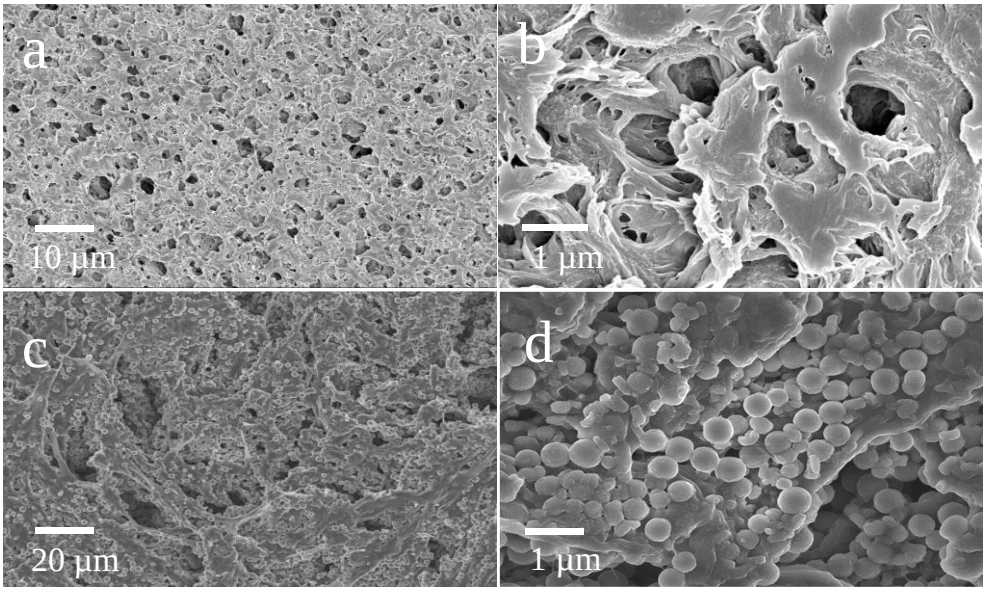


**Supplementary Fig. 2 SEM analysis**. **a-b** PVDF-HFP and **c-d** $SiO_2$/PVDF-HFP.

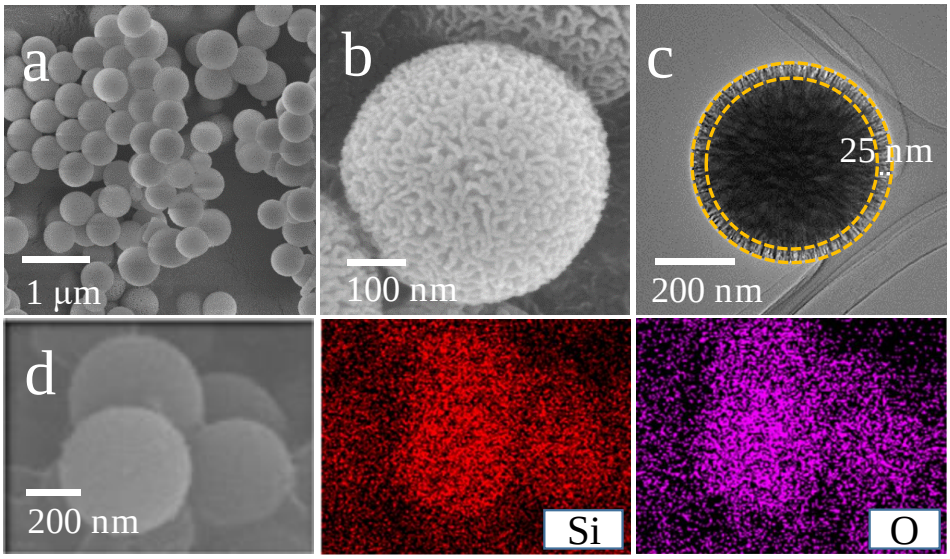


**Supplementary Fig. 3 Characterization of $SiO_2$ particles. a-b** SEM analysis; **c** TEM images; **d** EDS elemental mapping.

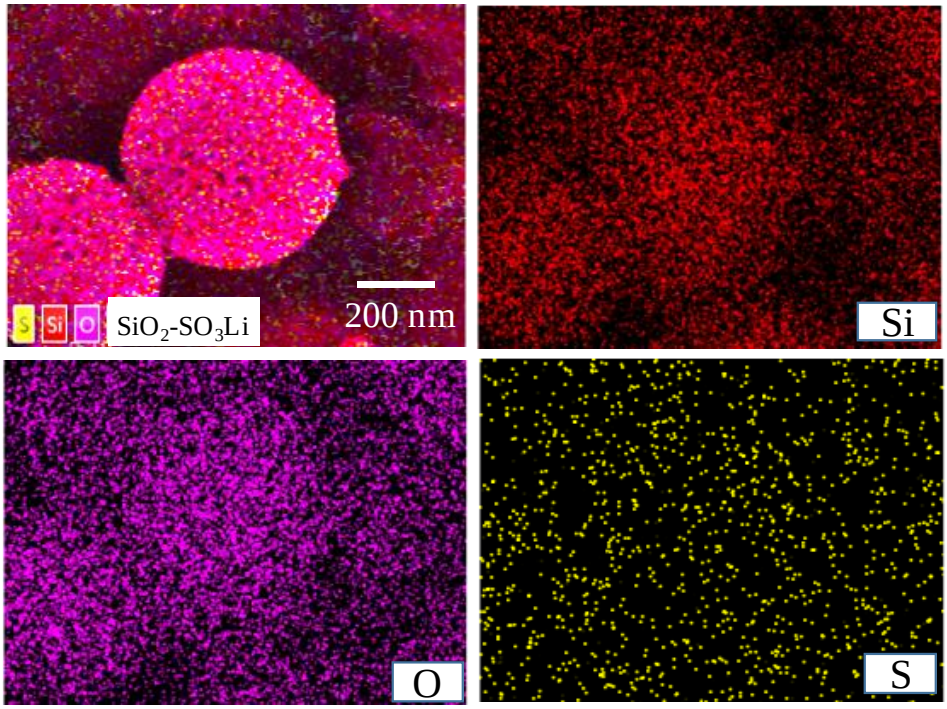


**Supplementary Fig. 4** EDS elemental mapping of $SiO_2$-$SO_3Li$ particles.

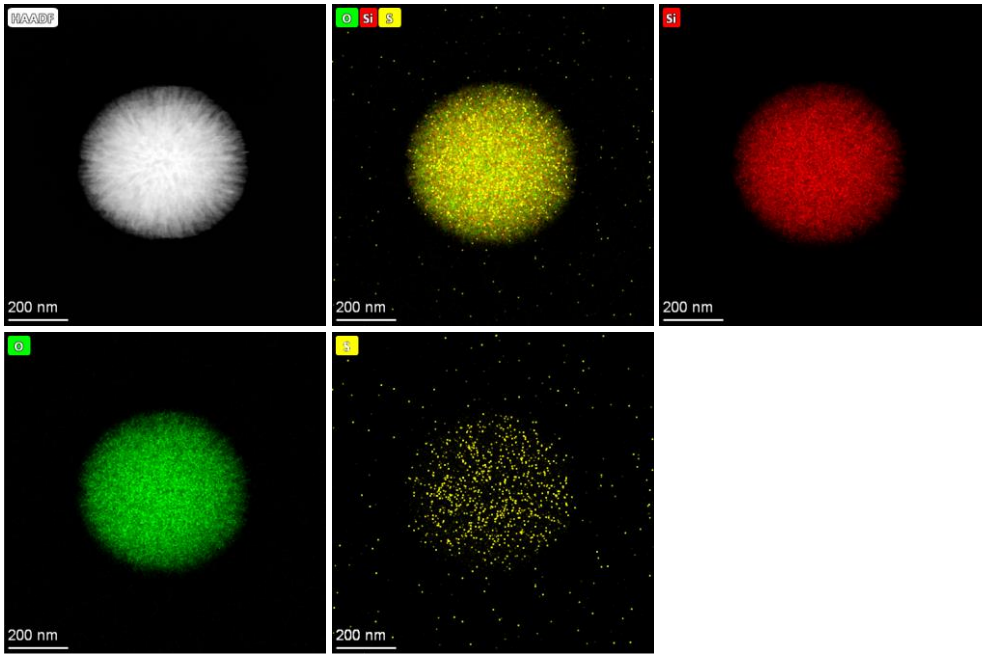


**Supplementary Fig. 5** HADDF-STEM images and the corresponding elemental mapping of $SiO_2$-$SO_3Li$ particles.

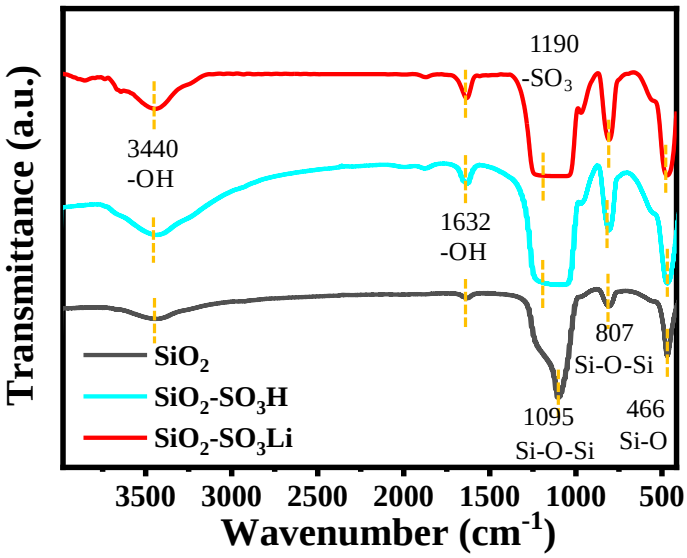


**Supplementary Fig. 6** FTIR spectra of porous $SiO_2$, $SiO_2$-$SO_3H$ and $SiO_2$-$SO_3Li$ nanoparticles.

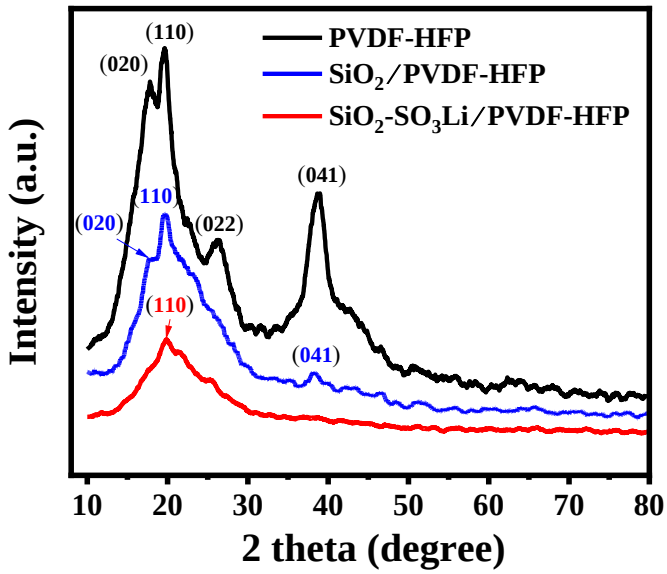


**Supplementary Fig. 7** XRD analysis


**Supplementary Fig. 8. Contact angle between polymer film and liquid electrolyte (1 M LiTFSI/TEGDME): a** PVDF-HFP; **b** $SiO_2$/PVDF-HFP; **c** $SiO_2$-$SO_3Li$/PVDF-HFP.

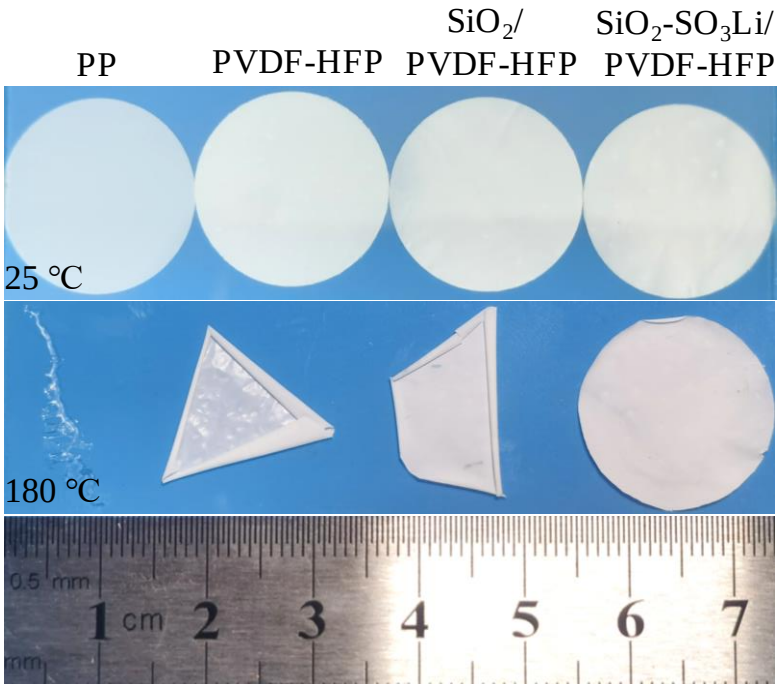


**Supplementary Fig. 9.** Digital photos before and after heating at 180 ℃ for 1 h.

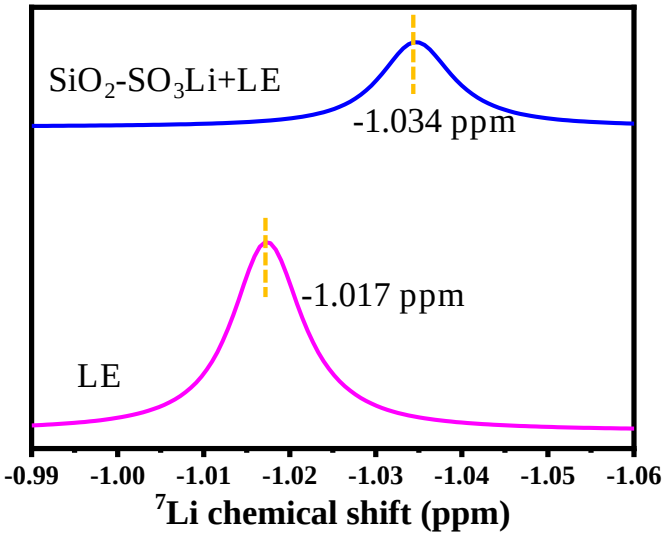


**Supplementary Fig. 10.** NMR analysis of $^{7}$Li chemical shift. The rose line represents liquid electrolyte (LE) and blue line represents $SiO_2$-$SO_3Li$ dipped in LE.

**Supplementary Note 1.**

The high $Li^+$ conductivity of quasi-solid electrolyte $SiO_2$-$SO_3Li$/PVDF-HFP at room temperature can be mainly attributed to the plenty of liquid electrolyte LiTFSI/TEGDME inside and $Li^+$-conductive groups -$SO_3Li$.

1) The electrolyte uptake of $SiO_2$-$SO_3Li$/PVDF-HFP reaches 380 wt% the dead weight, which is dominant the $Li^+$ conductivity.
2) Previous reports demonstrated that the sulfonate groups -$SO_3Li$ with electronegativity can simultaneously facilitate access by the electrolyte to promote ion pair dissociation and increase the mobility of $Li^+$ [1]. Furthermore, -$SO_3Li$ sites also provide the lithium ion hopping pathways to improve $Li^+$ conductivity[2,3].
3) The polymer skeleton PVDF-HFP provides a certain amount of $Li^+$ driving force through its segmental motion.

Therefore, the NNFQSE $SiO_2$-$SO_3Li$/PVDF-HFP with semi-dry surface can be seen as a “liquid electrolyte” to some extent, which exhibits high ion conductivity $5.4\times10^{-3}$ S/cm at room temperature, equivalent to the reported conventional liquid electrolyte LiTFSI/TEGDME[4].

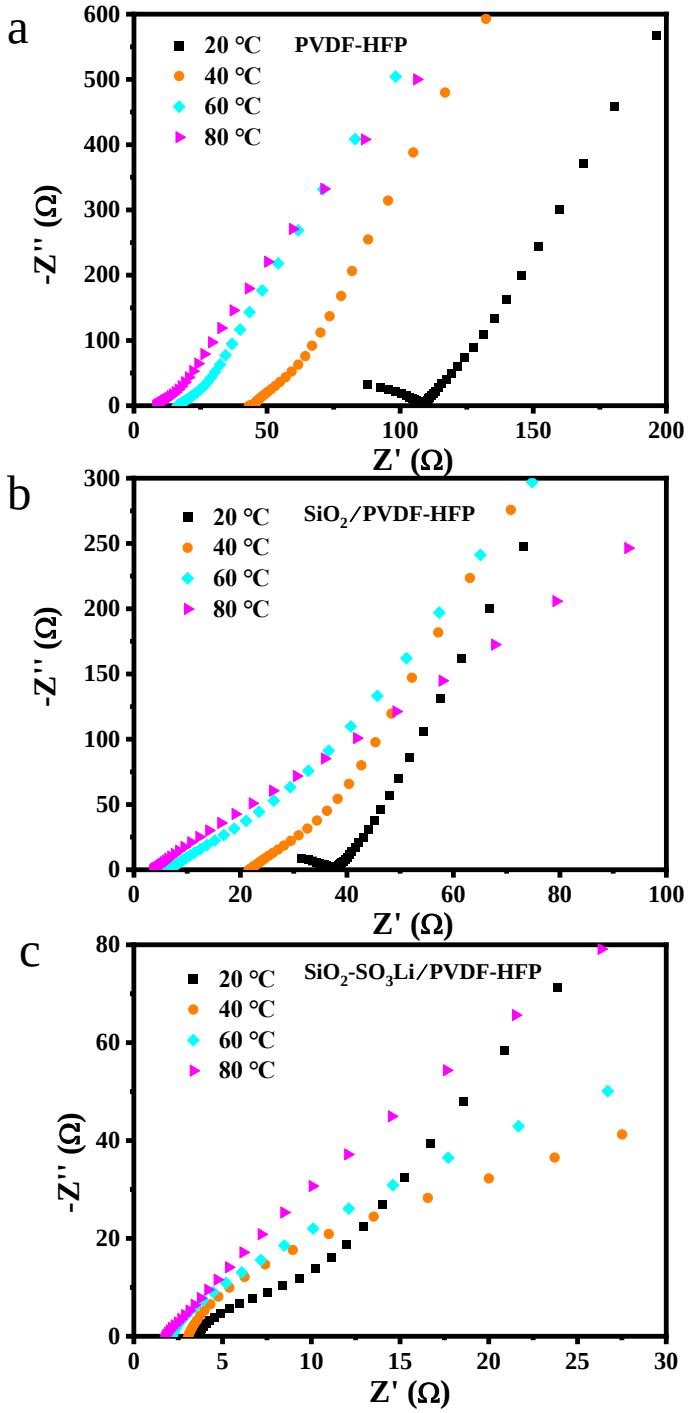


**Supplementary Fig. 11** EIS Nyquist plots at different temperatures.

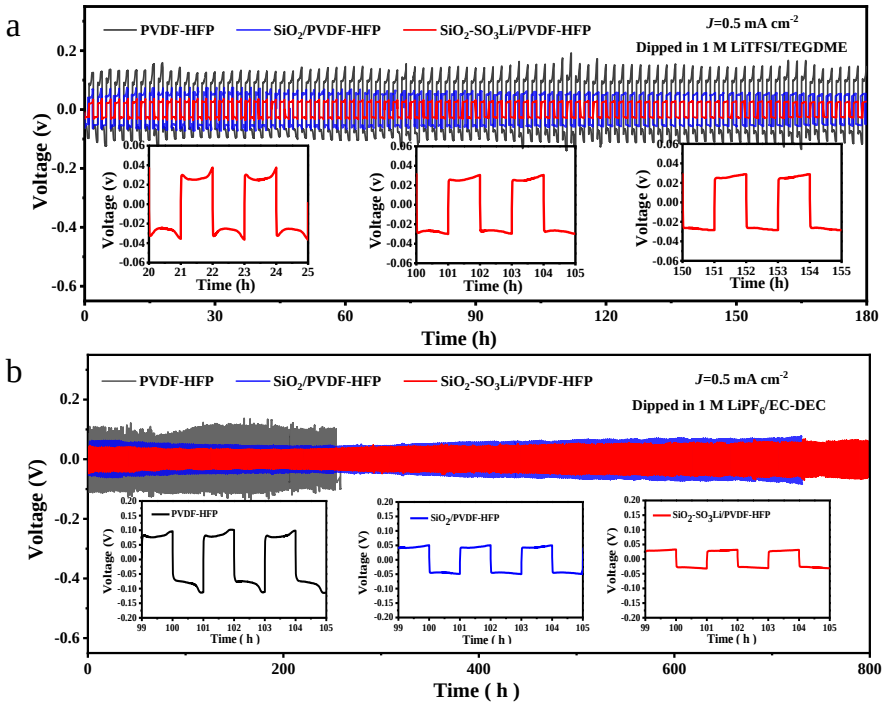


**Supplementary Fig. 12** Symmetric lithium batteries with quasi-solid electrolytes at a current density of 0.5 mA $cm^{-2}$ at 25 °C. **a** Dipped in 1 mol $L^{-1}$ LiTFSI/TEGDME, and the inserts are selected voltage profiles for different time; **b** Dipped in 1 mol $L^{-1}$ $LiPF_6$/EC-DEC, and the inserts are three kinds of voltage profiles at the same time for comparison.

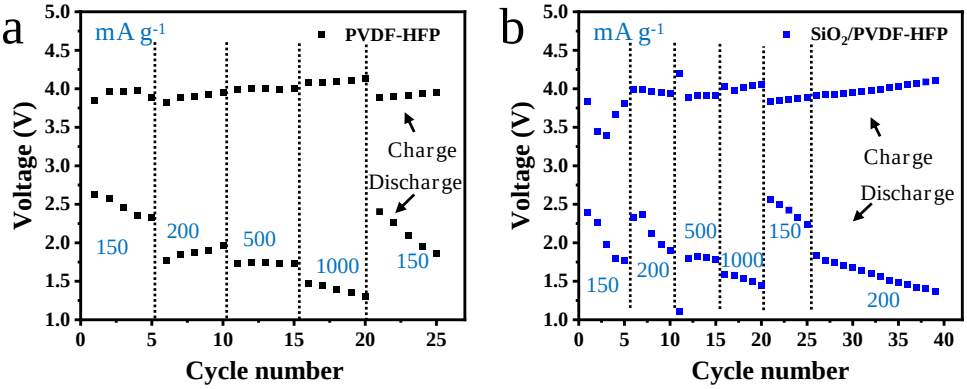


**Supplementary Fig. 13** Rate performances of Li-$O_2$ cells with **a** PVDF-HFP and **b** $SiO_2$/PVDF-HFP.

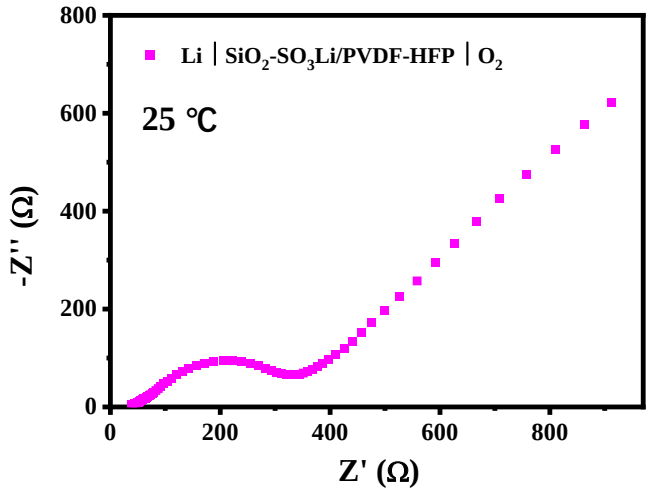


**Supplementary Fig. 14** EIS curve of Li | $SiO_2$-$SO_3Li$ /PVDF-HFP | $O_2$ after cycling.

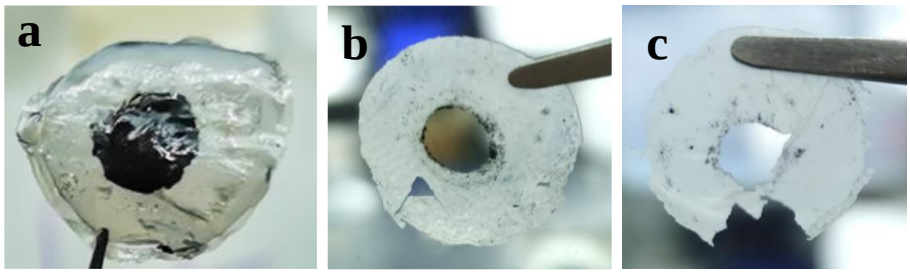


**Supplementary Fig. 15 Digital photos after cycling**. **a** $SiO_2$-$SO_3Li$/PVDF-HFP; **b** $SiO_2$/PVDF-HFP; **c** PVDF-HFP.

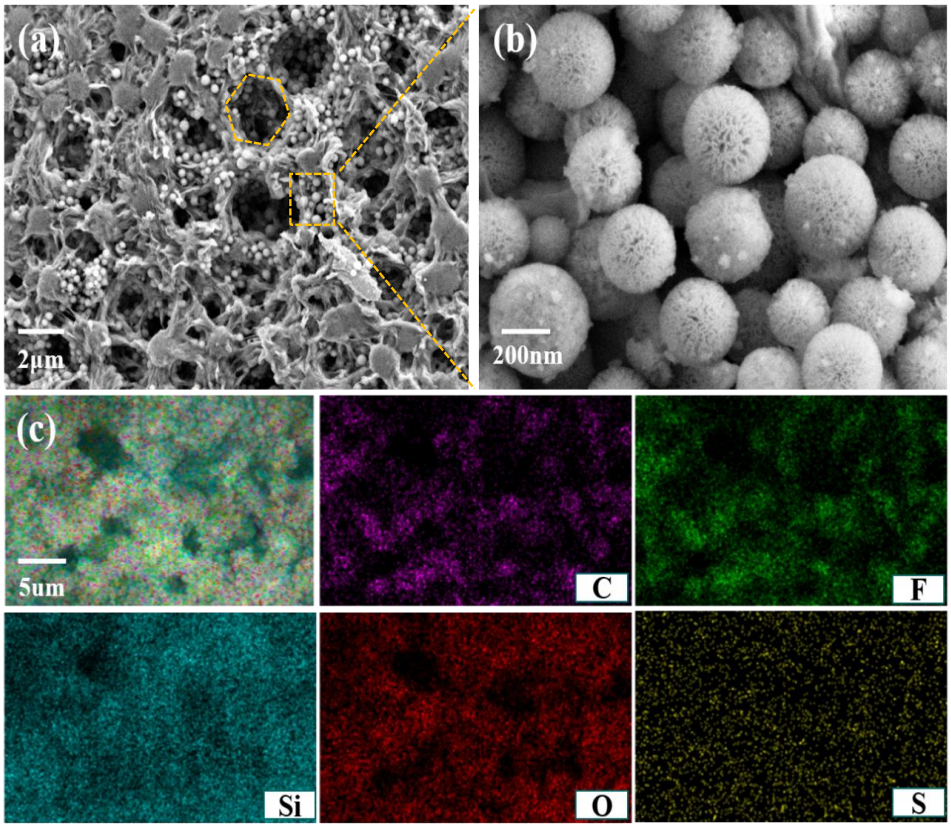


**Supplementary Fig. 16** The bird view of SEM analysis and EDS elemental mapping of $SiO_2$-$SO_3Li$/PVDF-HFP after 5000 h Li-$O_2$ cycling.

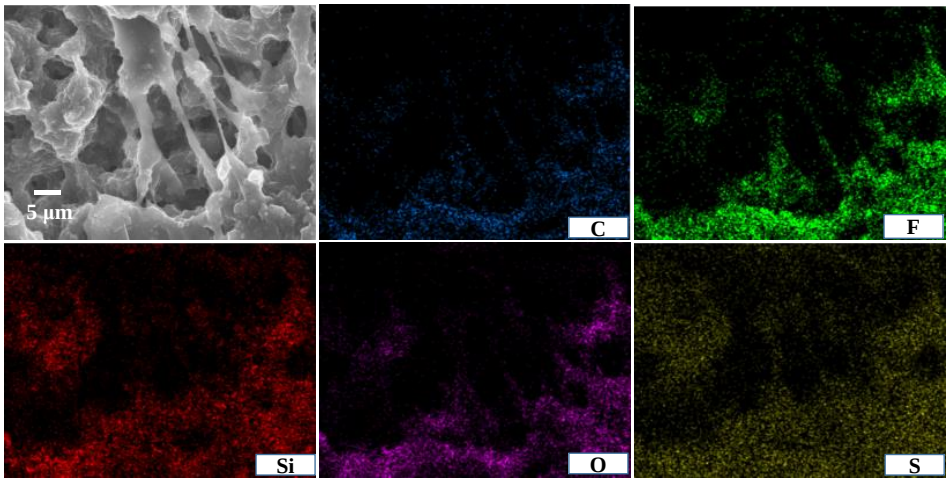


**Supplementary Fig. 17** Cross section EDS elemental mapping of $SiO_2$-$SO_3Li$ /PVDF-HFP after 5000 h Li-$O_2$ cycling.

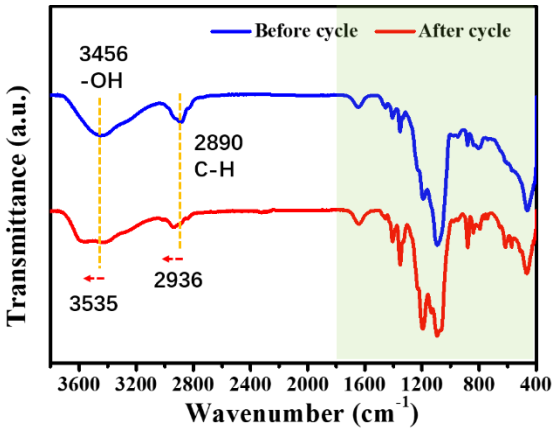


**Supplementary Fig. 18** FTIR spectra of NNFQSE $SiO_2$-$SO_3Li$/PVDF-HFP before and after 5000 h cycling.

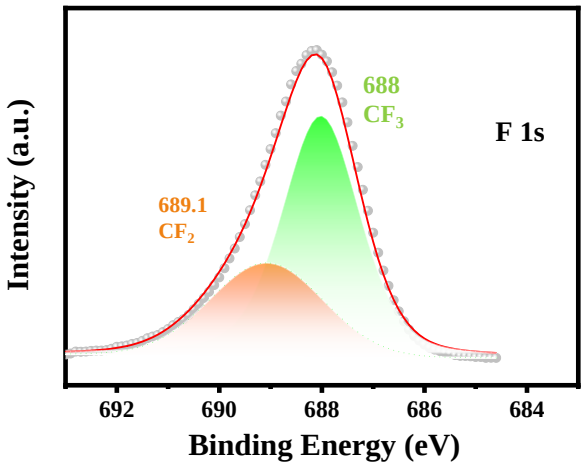


**Supplementary Fig. 19** F 1s XPS analysis of NNFQSE $SiO_2$-$SO_3Li$/PVDF-HFP before absorbing liquid electrolyte.

**Supplementary Note 2.**

After long-term cycling, the lithium anode surface of Li | $SiO_2$-$SO_3Li$/PVDF-HFP | $O_2$ exhibits bright with metallic luster (Supplementary Fig. 20a), and its SEM morphology shows smooth without obvious dendrite growth (Supplementary Fig. 20d-e). While the anode of Li | $SiO_2$/PVDF-HFP | $O_2$ turns black (Supplementary Fig. 20b) and appears rough surface (Supplementary Fig. 20f-g). And the lithium anode of Li | PVDF-HFP | $O_2$ turns pulverized (Supplementary Fig. 20c).

For cathode, in order to better understand how the $SiO_2$-$SO_3Li$/PVDF-HFP electrolyte affects the growth and decomposition of discharge products, we investigated the morphology and crystal structure of the cathode after discharge and charge. As shown in Supplementary Fig. 23, high-magnification SEM images reveal that the discharge products of $Li_2O_2$ are formed on the cathode (Supplementary Fig. 23a-b) and completely disappeared after charging (Supplementary Fig. 23c-d), demonstrating good reversibility during the charge/discharge process. Moreover, X-ray diffraction (XRD) analyses of the pristine, discharged, and charged cathodes were carried out in Supplementary Fig. 23e. The discharged cathode exhibits two weak peaks located at 32.9° and 35.8°, which correspond to the (100) and (101) crystal surfaces of $Li_2O_2$, respectively[5]. After charging, the peaks completely disappear and recover to be consistent with the pristine crystal structure. These results perfectly validate the $SiO_2$-$SO_3Li$/PVDF-HFP electrolyte exhibits robust chemical stability against products during cycling[6].

In addition, after 5000 h cycling, the cathode of Li | $SiO_2$-$SO_3Li$/PVDF-HFP | $O_2$ still maintains hollow tubular structure and there only exists little residue of solid-state products (Supplementary Fig. 24a). In contrast, the cathode structure of control groups becomes deformation or even collapsed, and there also filled with residue, which hinders the persistent cycling (Supplementary Fig. 24b-c). These results further

confirm that the NNFQSE $SiO_2$-$SO_3Li$/PVDF-HFP can trap the liquid electrolyte inside to prevent the side reaction with cathode and reduce the residue of solid-state products.

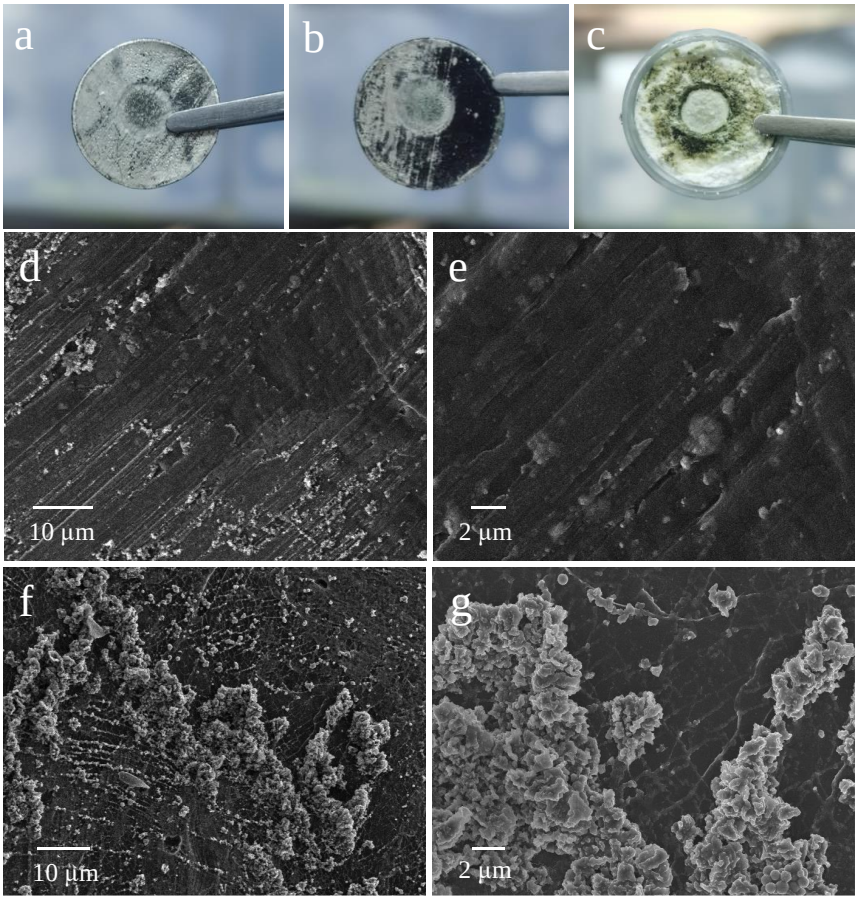


**Supplementary Fig. 20 Digital photos and surface morphologies of Li anodes after cycling**. **a, d, e** Li | $SiO_2$-$SO_3Li$/PVDF-HFP | $O_2$; **b, f, g** Li | $SiO_2$/PVDF-HFP | $O_2$; **c** Li | PVDF-HFP | $O_2$.

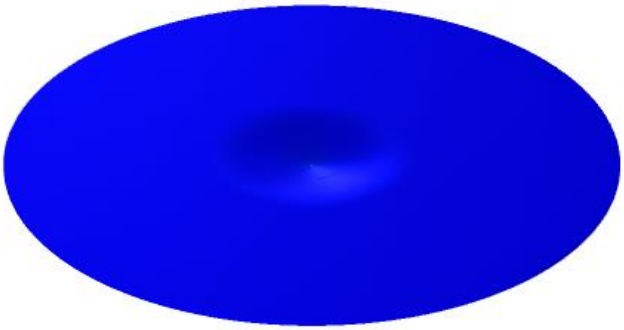

**Supplementary Fig. 21** COMSOL simulation of the NNFQSE's deformation.

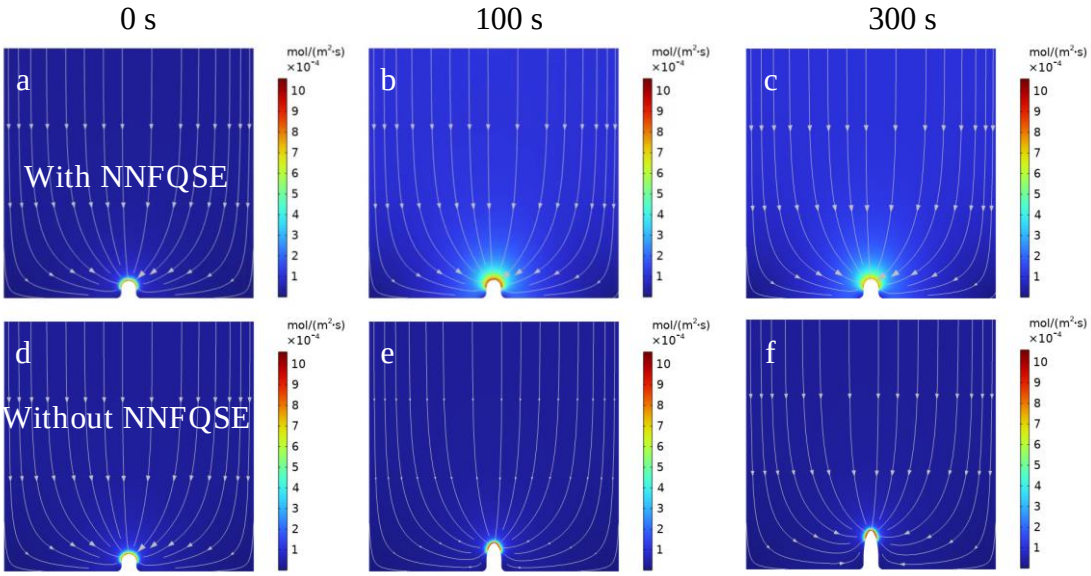


**Supplementary Fig. 22**. Ionic flux and Li dendrite growth simulations during prolonged time of 300 s **a-c** with NNFQSE or **d-e** without NNFQSE.

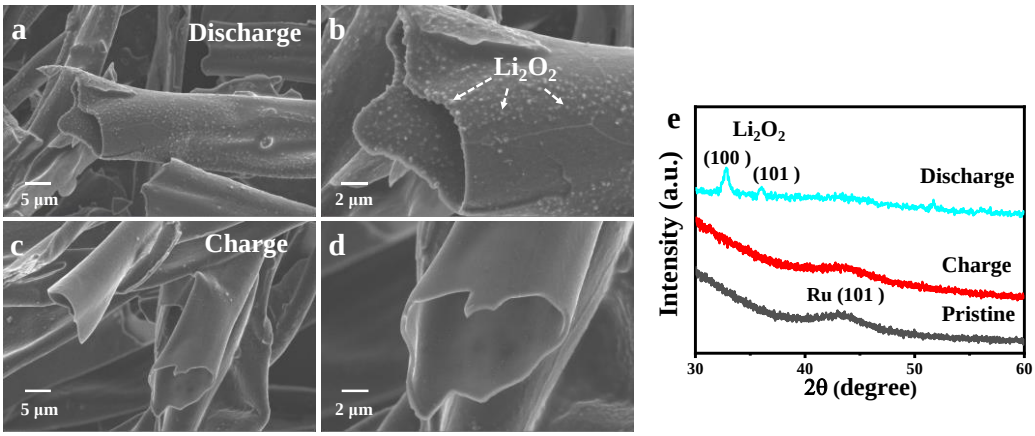


**Supplementary Fig. 23 Characterization of the growth and decomposition of discharge products. a-b** SEM images showing the $Li_2O_2$ is formed on the cathode after discharge; **c-d** SEM images showing the $Li_2O_2$ formed on the cathode has vanished after charge. **e** XRD analysis of cathode after discharge and charge.

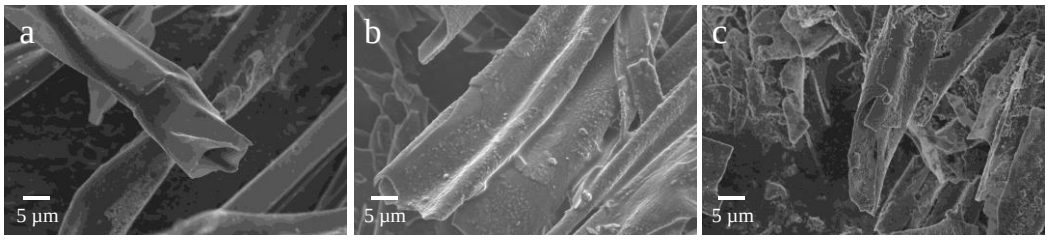


**Supplementary Fig. 24 Surface morphologies of cathode after cycling**. **a** Li | $SiO_2$-$SO_3Li$/ PVDF-HFP | $O_2$; **b** Li | $SiO_2$/PVDF-HFP | $O_2$; **c** Li | PVDF-HFP | $O_2$.

**Supplementary Table 1.** Porous features of PVDF-HFP, $SiO_2$/PVDF-HFP and $SiO_2$-$SO_3Li$/PVDF-HFP.

| Electrolyte | Porosity ratio (%) | Volume density ($g\ ml^{-1}$) | Apparent (skeleton) density ($g\ ml^{-1}$) | Total pore volume ($mL\ g^{-1}$) | Total pore area ($m^2\ g^{-1}$) |
|---|---|---|---|---|---|
| PVDF-HFP | 74.6 | 0.34 | 1.34 | 2.19 | 7.57 |
| $SiO_2$ /PVDF-HFP | 58.4 | 0.59 | 1.43 | 0.98 | 16.06 |
| $SiO_2$-$SO_3Li$ /PVDF-HFP | 62.9 | 0.48 | 1.28 | 1.32 | 18.27 |

**Supplementary References**


1 Xu, J. *et al.* Towards High Performance Li-S Batteries via Sulfonate‐Rich COF - Modified Separator. *Adv. Mater.* **33**, 2105178, doi:10.1002/adma.202105178 (2021).

2 Cao, Y. *et al.* Ion Selective Covalent Organic Framework Enabling Enhanced Electrochemical Performance of Lithium−Sulfur Batteries. *Nano Lett.* **21**, 2997−3006, doi:10.1021/acs.nanolett.1c00163 (2021).

3 Jeong, K. *et al.* Solvent-Free, Single Lithium-Ion Conducting Covalent Organic Frameworks. *J. Am. Chem. Soc.* **141**, 5880−5885, doi:10.1021/jacs.9b00543 (2019).

4 Qiao, L. X. *et al.* Stable non-corrosive sulfonimide salt for 4-V-class lithium metal batteries. *Nat. Mater.* **21**, 455–462, doi:10.1038/s41563-021-01190-1 (2022).

5 Song, H. *et al.* Hierarchically Porous, Ultrathick, "Breathable" Wood‐Derived Cathode for Lithium‐Oxygen Batteries. *Advanced Energy Materials* **8**, 1701203 (2018).

6 Wu, Z. Z. *et al.* Evolving aprotic Li–air batteries. *Chem. Soc. Rev.* **51**, 8045, doi:10.1039/D2CS00003B ( 2022).